Electronic Supplementary Information

Coupled Defect Chemistry and Redox dynamics in Bismuth Gahnite System for Self-Adaptive Tribological Interfaces

Saithathul Fathima Sameera, [†a] Najiya Nasirin, [†a] Dalaver H Anjum,[b] Sheik Muhammadhu Aboobakar Shibli[*a,c]

[a] Department of Chemistry, University of Kerala, Kariavattom Campus, Thiruvananthapuram, Kerala – 695 581, India

[b] Physics Department, Khalifa University, Abu Dhabi 127788, United Arab Emirates

[c] Centre for Renewable Energy and Materials, University of Kerala, Kariavattom Campus, Thiruvananthapuram- Kerala – 695 581, India

† These authors contributed equally to this work and share first authorship

Corresponding Author: *E-mail address: smashibli@yahoo.com

(Sheik Muhammadhu Aboobakar Shibli)

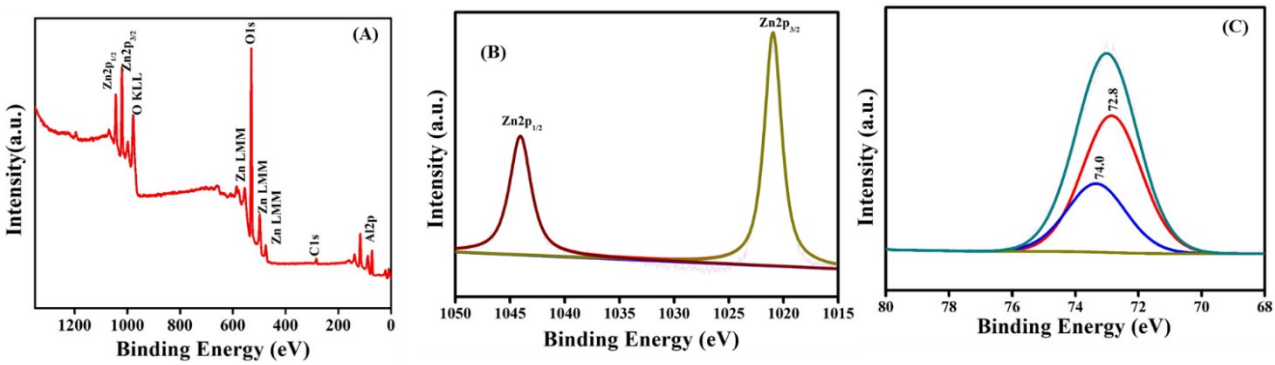

Fig. S1 (A) XPS survey spectrum of ZA, high resolution images of (B) Zn2p (C) Al2p

The presence of Zn atoms in the oxidized state Zn^{2+} ion is confirmed by the Zn 2p core level spectrum's two BE peaks, which are centered at 1020.8 eV and 1043.9 eV, respectively, and correspond to doublets Zn $2p_{3/2}$ and Zn $2p_{1/2}$.[1]

It is evident that the Al 2p peak is made up of a single peak that is located at 72.8and 74.0 eV, respectively. The octahedral location of Al in the $ZnAl_2O_4$ lattice, or Al in the AlO_6 octahedra, is the source of this peak.[2]

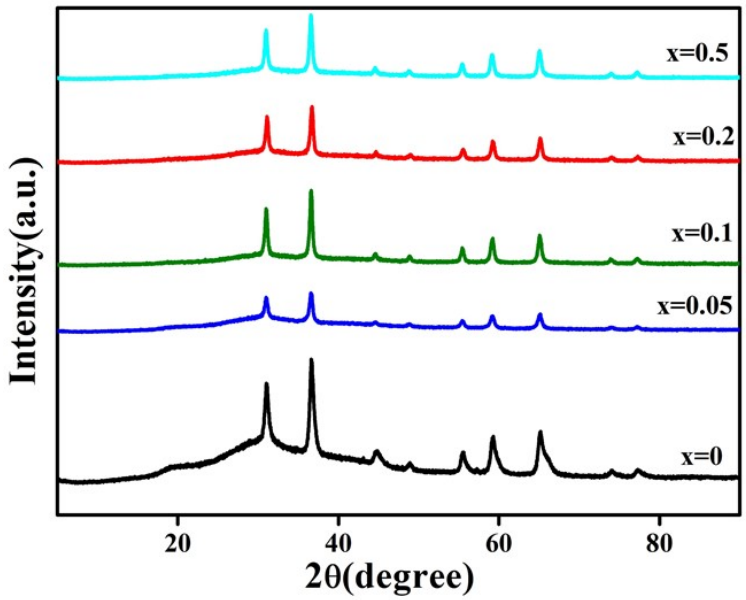

Fig. S2 Stacked XRD spectra of all prepared samples

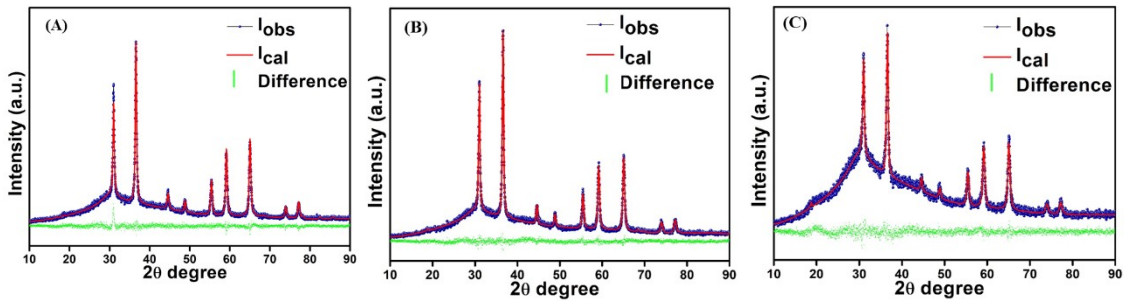

Fig. S3 Graphical output of the Rietveld refinement of (A) $ZAB_{0.05}$ (B) $ZAB_{0.10}$ (C) $ZAB_{0.50}$

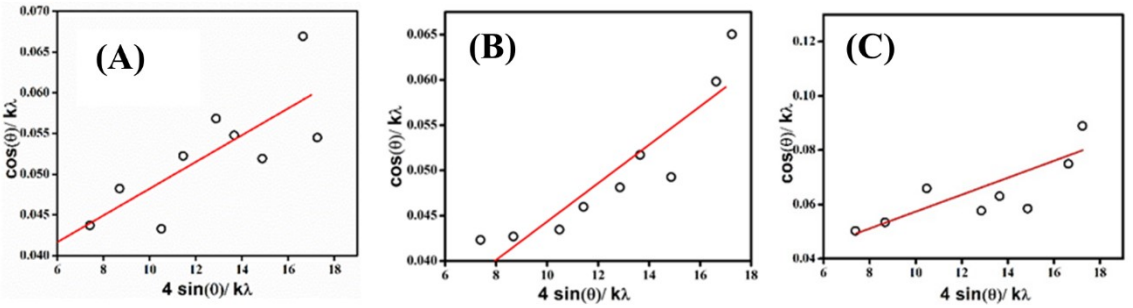

Fig. S4 W-H plot of (A) $ZAB_{0.05}$ (B) $ZAB_{0.10}$ (C) $ZAB_{0.50}$

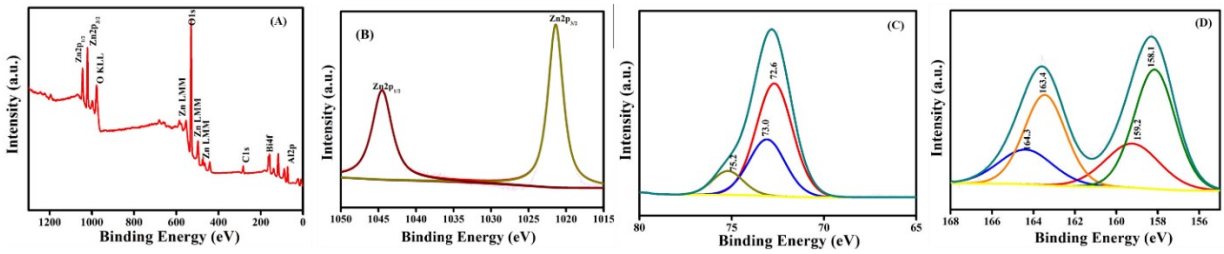

Fig. S5 (A)XPS Survey spectra of $ZAB_{0.20}$, High resolution spectra of (B) Zn2p (C) Al2p (D) Bi4f

Bi 4f fine scan spectrum deconvolute into four peaks. The Bi $4f_{5/2}$ and Bi $4f_{7/2}$ of positively charged Bi species (Bi^{3+}) are responsible for the two peaks at 164.4 and 159.1 eV, whereas the Bi $4f_{5/2}$ and Bi $4f_{7/2}$ of metallic Bi (Bi^{0}) are responsible for the other two peaks at 162.7 and 157.3 eV.[3]

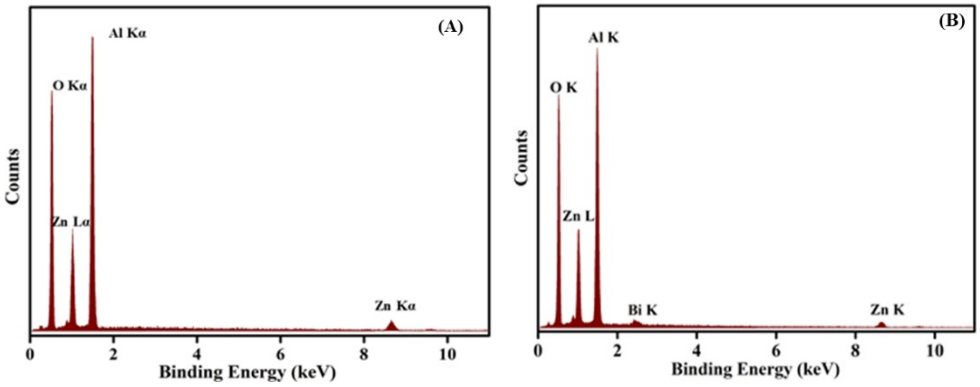

Fig. S6 EDX spectrum of (A) ZA (B) $ZAB_{0.20}$

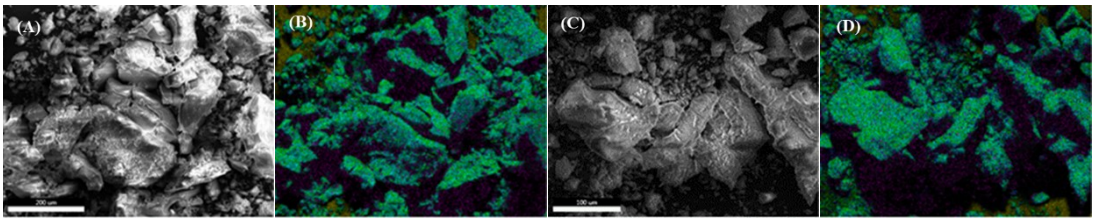

Fig. S7 (A)Selected Area for mapping of ZA, (B) Element overlay of ZA, (C) Selected Area for mapping of $ZAB_{0.20}$ (D) Element overlay of $ZAB_{0.20}$

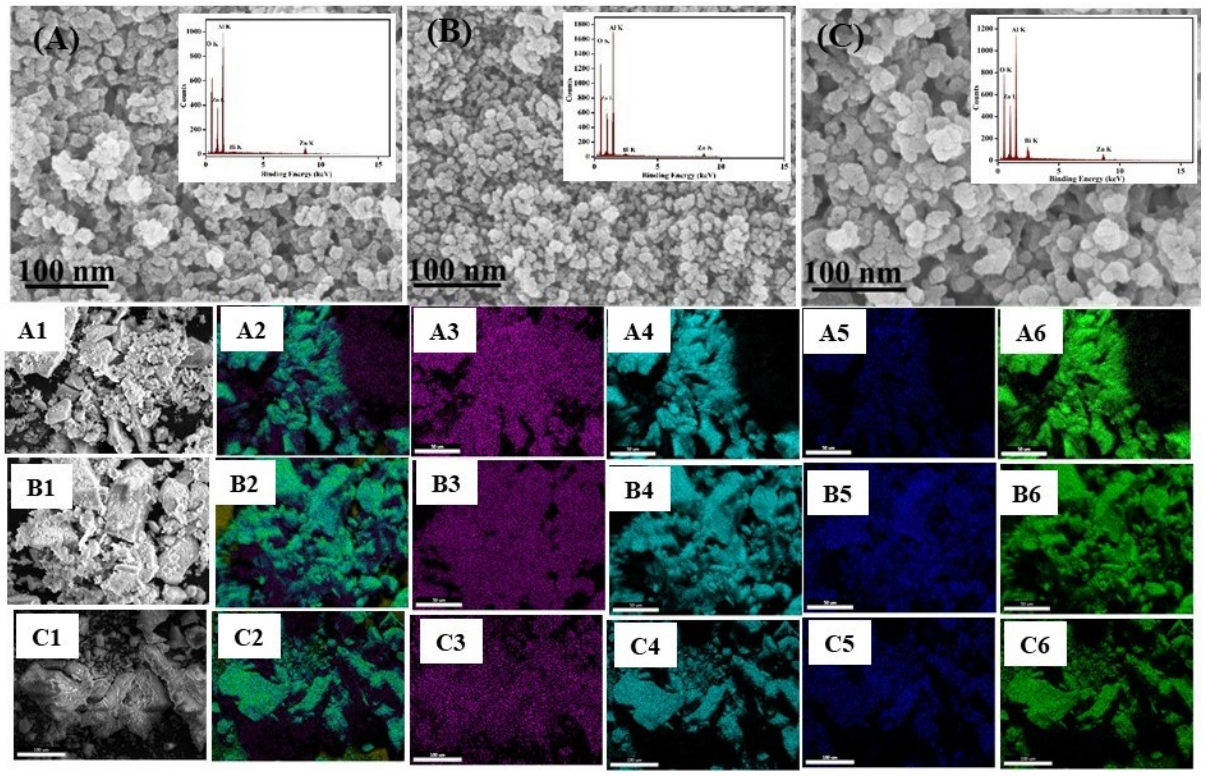

Fig. S8 FESEM micrographs of (A) $ZAB_{0.05}$ (B)$ZAB_{0.10}$ (C)$ZAB_{0.50}$, inset showing corresponding EDX spectra and corresponding mapping of (A1-C1), (A2-C2), (A3-C3). (A4-C4), (A5-C5) & (A6-C6) are the selected area for EDX mapping, overlay of elements, Zn scan, Al scan, Bi scan and O scan respectively.

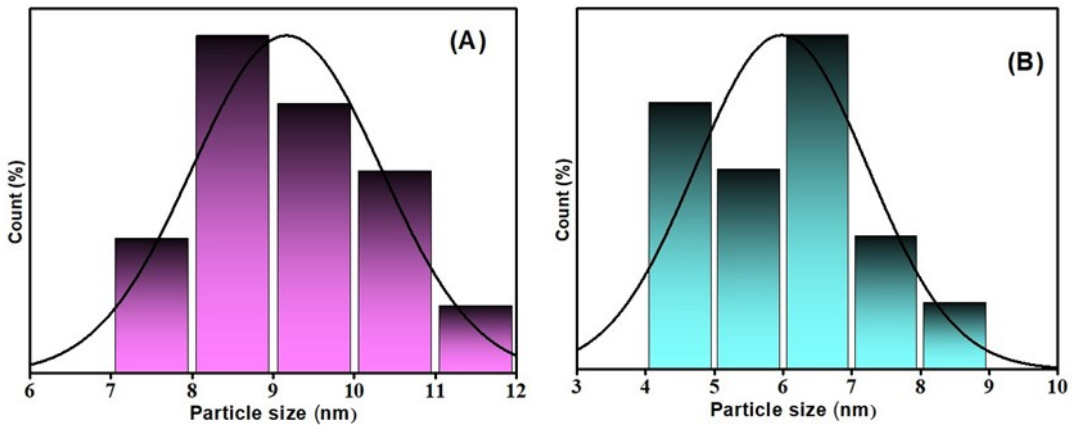

Fig. S9 Histogram of particle size distribution from TEM measurement of (A) ZA and (B) $ZAB_{0.2}$.

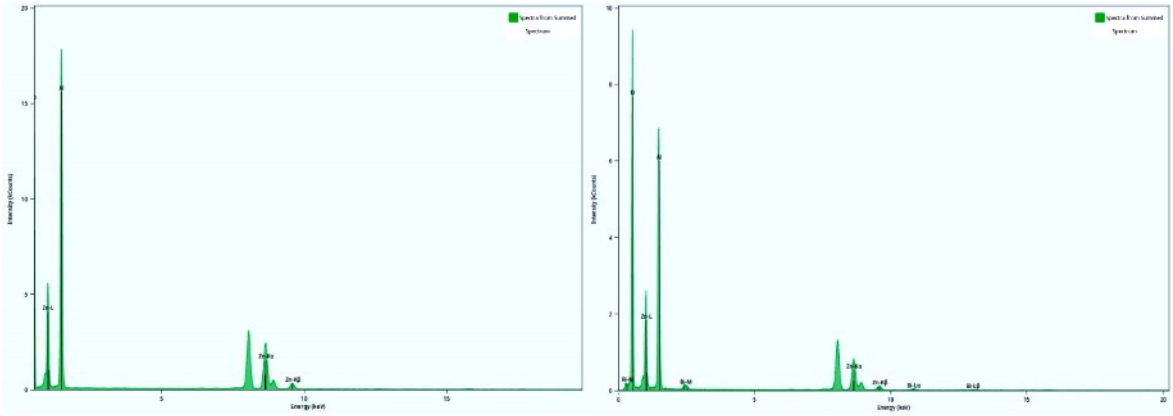

Fig. S10 TEM-EDS elemental analysis (A) ZAB, (B) $ZAB_{0.2}$

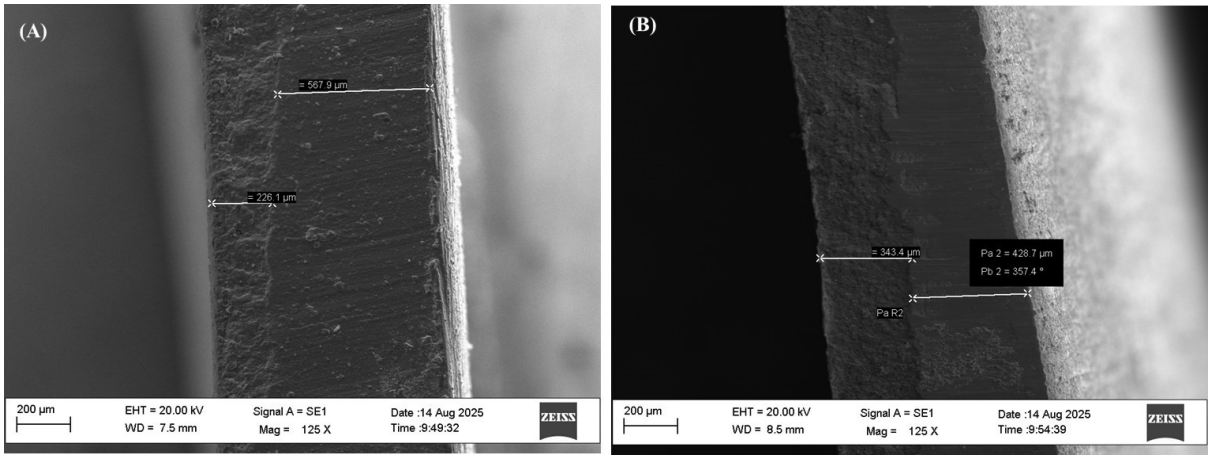

Fig. S11 Cross sectional SEM images of (A) NiP (B) $ZAB_{0.2}$@NiP

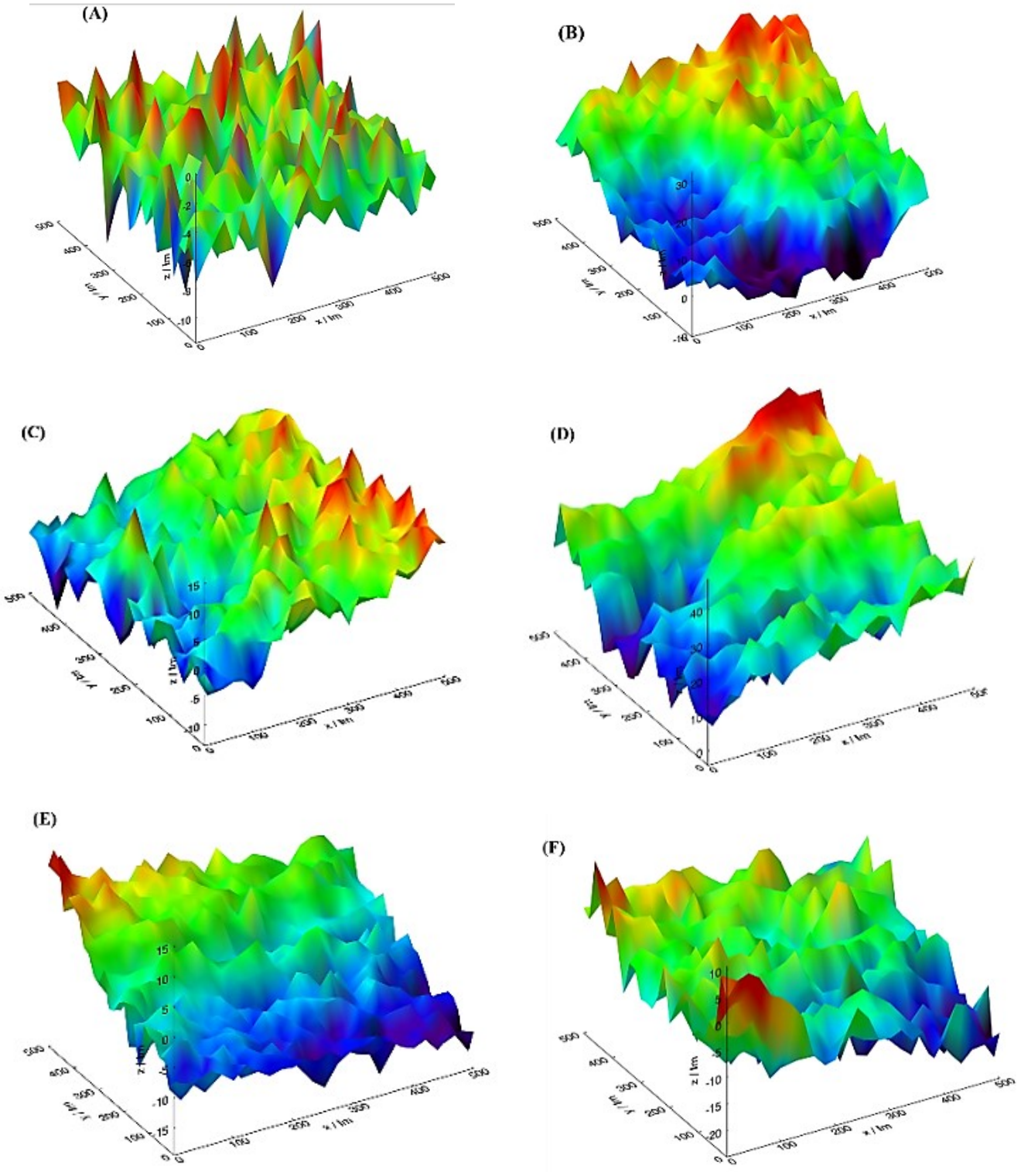
(A)
(B)
(C)
(D)
(E)
(F)
z / km
x / km
y / km

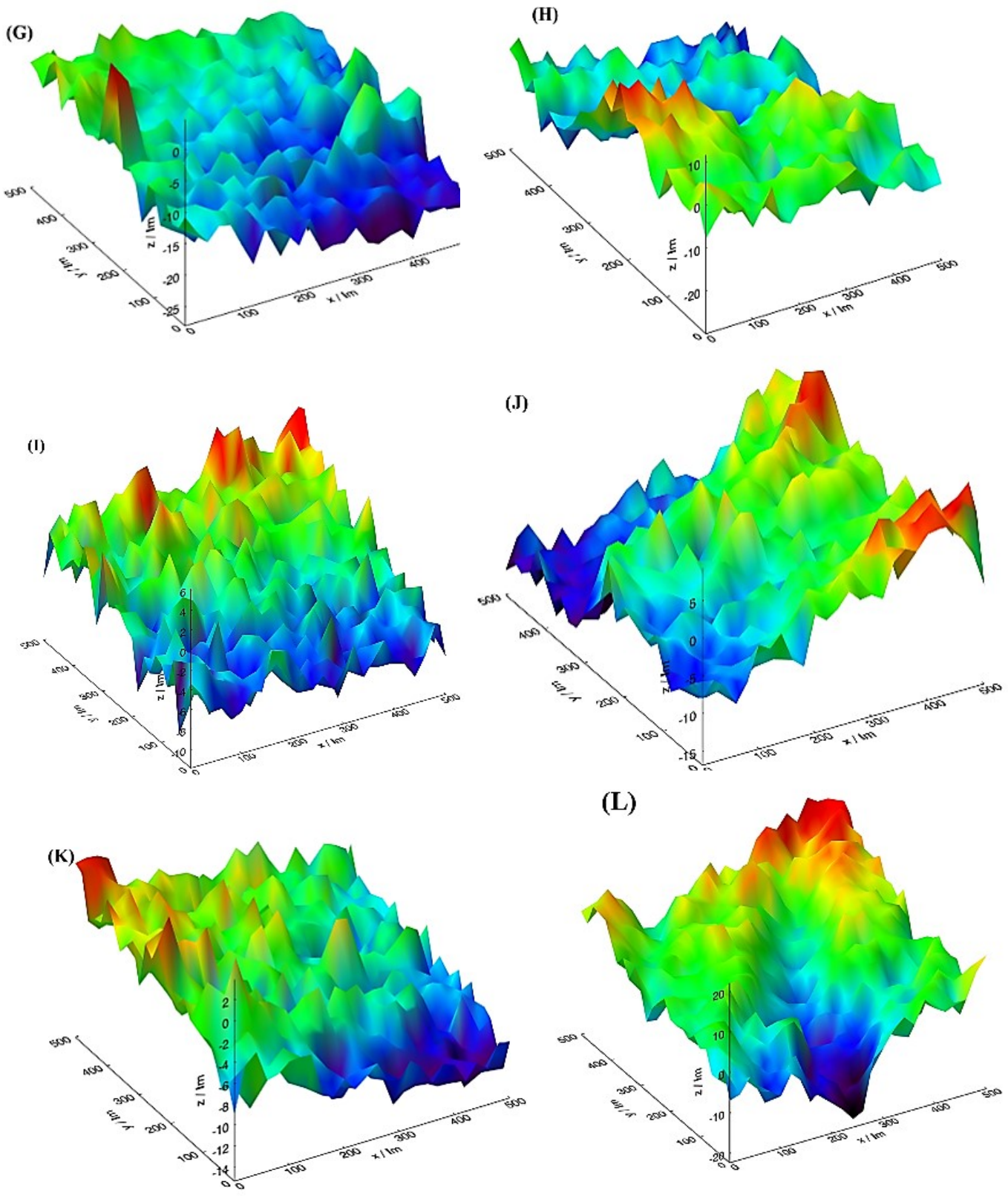

Fig. S12 OSP Images of (A,C,E,G,I &K) Outside wear track of NiP, ZA, $ZAB_{0.05}$, $ZAB_{0.10}$, $ZAB_{0.20}$ & $ZAB_{0.50}$ and (B,D,F,H,J& L) inside wear track NiP, ZA, $ZAB_{0.05}$, $ZAB_{0.10}$, $ZAB_{0.20}$ & $ZAB_{0.50}$

Sa Arithmetic average height of the surface (μm)

Sq root mean square height of the surface (μm)

Ssk Skewness of height distribution (dimensionless)

Sku Kurtosis of height distribution (dimensionless)

Sp maximum surface peak Height (μm)

Sv maximum valley depth (μm)

St maximum surface vertical peak-to-valley height (μm)

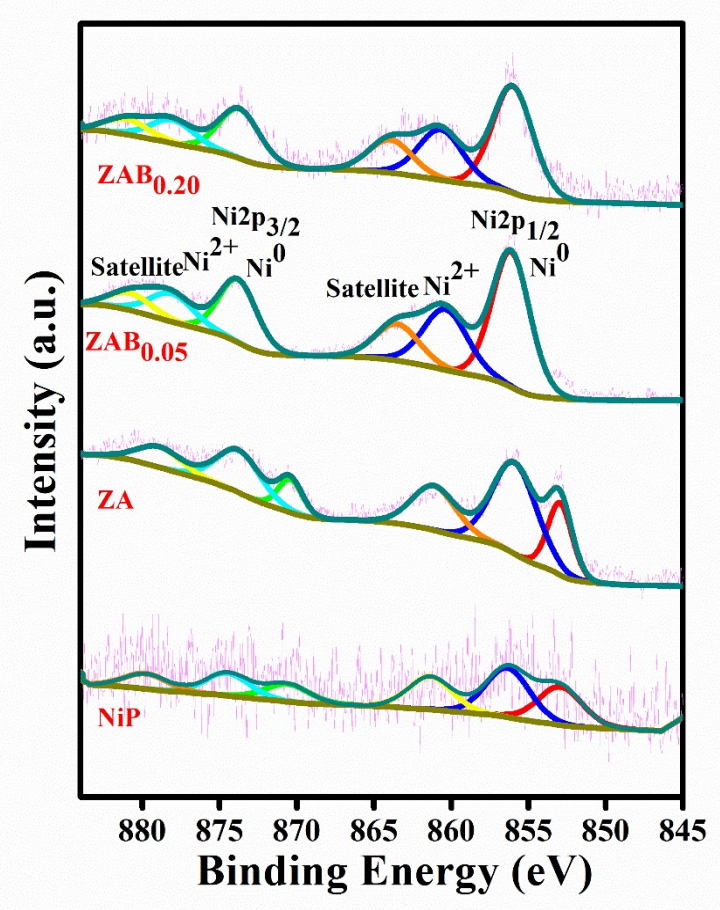

Fig. S13 High resolution image of (A) Ni2p outside wear track

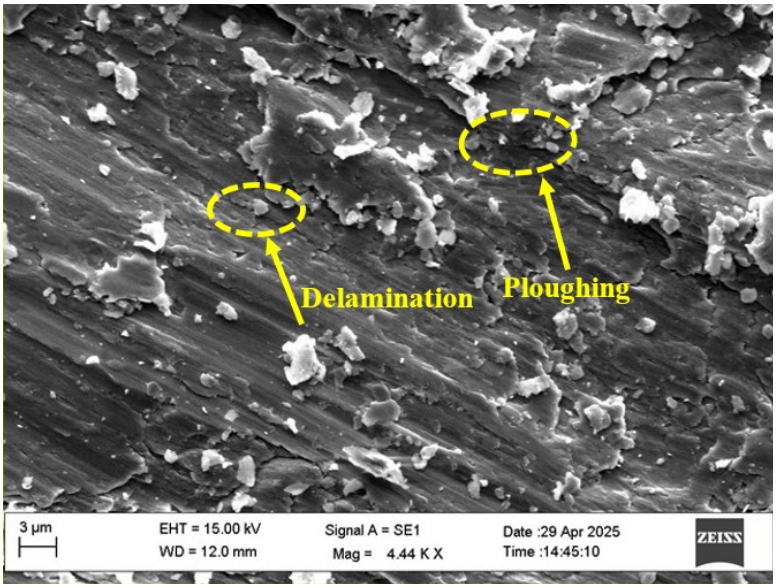

Fig. S14 (A) SEM image of $ZAB_{0.5}$ inside wear track

When the bismuth concentration increases to x=0.5 in $ZnAl_{2-x}Bi_xO_4$ in the $ZAB_{0.5}$@NiP matrix, the excess bismuth starts segregating to grain boundaries and interfaces, where it forms weak Bi-rich intergranular layers. High-resolution studies in related systems have shown that such segregated Bi can reconstruct into bilayers or ordered interfacial phases with very low cohesive strength.[4] The alterations in the chemical state and crystal structure of zinc aluminate induced by bismuth changes the frictional behaviour, resulting in pronounced changes in frictional response during sliding.[5] At high concentrations of bismuth, the accumulation of bismuth atoms along grain boundaries can cause embrittlement, leading to metallurgical fracture.[6] These regions fracture readily during sliding, generating loose debris and prevents the development of a stable, protective tribofilm. From the SEM image (Fig.S14) of the $ZAB_{0.5}$ worn track, it is evident thet fragmented particles, delamination, and discontinuous smearing has occurred. The brittle failure of these bismuth-rich zones and the formation of third-body debris lead to the observed rise in friction and wear (COF=0.70).

Table S1. Structure refinement values obtained by Rietveld refinement

Samples	ZAB	$ZAB_{0.05}$	$ZAB_{0.10}$	$ZAB_{0.20}$	$ZAB_{0.50}$
a(Å)	8.1446	8.1370	8.1326	8.1094	8.1416
V(Å)^3	540.26	538.76	537.88	533.29	539.67
Space group	*Fd3m*	*Fd3m*	*Fd3m*	*Fd3m*	*Fd3m*
R_{exp}(%)	6.50	6.89	6.67	6.60	6.37
R_{wp}(%)	7.35	8.00	7.70	9.02	7.13
R_p(%)	5.63	6.18	5.74	7.06	5.41
GOF	1.13	1.16	1.15	1.37	1.12

R_{exp} represents the statistically expected R-factor based on data quality and number of refinable parameters. It provides a reference to compare the achieved fit.

R_{wp} -The difference between the calculated and actual diffraction intensity is termed as the weighted profile residual factor.

R_p measures the discrepancy between the observed and calculated diffraction profiles. Lower $R_p$indicates better agreement.

Goodness of fit (GOF) is used as a metric to evaluate the optimised Rietveld refinement results which is defined as follows:

$$\text{GOF}= \frac{\sum_i \omega_i \left(y_i^{Obs} - y_{x,i}^{Calc}\right)^2}{N_{obs} - p}$$

where *x* represents a fixed parameter configuration of Rietveld refinement including the scope of the refinement, y_i^{Obs} is the i-the observed diffraction intensity, $y_{x,i}^{Calc}$ is the diffraction intensity calculated using the physical model with the configuration *x*, and ω_i be the weight corresponding to the inverse of the uncertainty of i-th intensity. N_{obs} is the number of data points of observed XRD pattern, and *p* is the number of variables in the fitting model.

Table S2 TEM-EDS elemental composition

	ZAB		$ZAB_{0.2}$	
	Atomic Percent	**Mass Percent**	**Atomic Percent**	**Mass Percent**
Zn	7.34	20.31	5.47	15.87
Al	36.67	41.82	31.22	37.38
Bi	-	-	0.21	1.95
O	55.99	37.87	63.11	44.81

Table S3 Comparison of wear parameters of the host matrix and tuned coating

sample	Wear rate, k ($\times 10^{-5}$ mm^3/Nm)	COF	Vickers Hardness (HV)
NiP	12.736	0.93	116
ZA	7.407	0.72	122
$ZAB_{0.05}$	5.323	0.61	145
$ZAB_{0.1}$	2.762	0.42	188
$ZAB_{0.2}$	0.889	0.19	191
$ZAB_{0.5}$	6.674	0.70	126

Table S4 Comparative table with other wear resistant materials

Material	Wear rate	COF	Load	Year ref
Ni–P–Cr_3C_2	-	0.24	20 N	2024 [7]
Ni-P-8YSZ	$5.51 \pm 0.64(\times 10^{-6} mm^3$ /Nm)	0.40	-	2022 [8]
NiP + PTFE	$4.76\times10^{-8} mm^3$/N m	0.83	-	2005 [9]
5MAAF	5.4×10^{-6} mm^3 N^{-1} m^{-1}	0.39	-	2026 [10]
Cr–Fe–Al_2O_3	1.8×10^{-6} mm^3/N m	0.83	-	2024 [11]
h-BN/TiO_2-WO_3	4.29×10^{-5} mm^3/Nm	0.12	1 N	2025 [12]
`Ni–W–B/P-VC	9.578×10^{-8} mm^2/Nm	0.27	-	2024 [13]
TiAlMoN	0.849×10^{-6} mm^3/Nm	-	-	2024 [14]
Ni-B-0.5Gr	7.04×10^{-5} mm^3/Nm	1.15	-	2024 [15]
$ZAB_{0.2}$	0.889×10^{-5} mm^3 /Nm	0.19	20 N	Present work

References

(1) G. Dasi, T. Lavanya, S. Suneetha, S. Vijayakumar, J.-J. Shim and K. Thangaraju, Spectrochim. Acta, Part A, 2022, 265, 120377.
(2) M. Jain, Manju, R. Kumar, S. O. Won, K. H. Chae, A. Vij and A. Thakur, Sci. Rep., 2020, 10, 385.
(3) Y. Wan, H. Zhou, M. Zheng, Z.-H. Huang, F. Kang, J. Li and R. Lv, Adv. Funct. Mater., 2021, 31, 2100300.
(4) Z. Yu, P. R. Cantwell, Q. Gao, D. Yin, Y. Zhang, N. Zhou, M. P. Harmer et al., Science, 2017, 358, 97–101.
(5) S R. Schweinfest, A. T. Paxton and M. W. Finnis, Nature, 2004, 432, 1008–1011.
(6) Pablo, G. R., van den Nieuwenhuijzen Karin, J. H., Walter, L., & ten Elshof Johan, E. (2016).
(7) Q. Chen, S. Xu, Y. He, S. Yan, Y. Fan, Z. Li, H. Zhou, H. Li, K. Wei, X. Gong and X. Cheng, Langmuir, 2024, 40, 16400–16418.
(8) Y. He, S. Zhang, Y. He, R. Song, Z. Zhang, B. Liu, H. Li and J. Shangguan, Colloids Surf., A, 2022, 654, 130059.
(9) A. Ramalho and J. C. Miranda, Wear, 2005, 259, 828–834.
(10) K. Yu, Q. Cheng, J. Cheng, Y. Geng, S. Zhu, K. Zhang, S. Wan and J. Yang, J. Mater. Sci. Technol., 2026, 247, 14–28.
(11) A. A. Burkov, M. A. Kulik, A. Yu. Bytsura and M. A. Ermakov, J. Frict. Wear, 2023, 44, 346–353.
(12) Z. Li, Y. Wang, B. Wang, L. Zhao and M. Yuan, Langmuir, 2025, 41, 18081–18091.
(13) X. Gong, Y. He, L. Yan, H. Zhou, Y. He, K. Wei, Q. Chen and S. Xu, Langmuir, 2024, 40, 11670–11683.
(14) A. Belgroune, L. Aissani, A. Alhussein, M. Zaabat, A. Obrosov and S. Rtimi, ACS Appl. Eng. Mater., 2024, 2, 345–359.
(15) V. Niksefat and F. Mahboubi, Tribol. Int., 2024, 198, 109905.